A Predictive Model for the Pd-Catalyzed Site-Selective Oxidation of Diols

Marinus, Nittert; Eisink, Niek N H M; Reintjens, Niels R M; Dijkstra, Renger S; Havenith, Remco W A; Minnaard, Adriaan J; Witte, Martin D

Published in:
Chemistry – A European Journal

DOI:
10.1002/chem.202300318

Publication date:
2023

Chemistry–A European Journal
Research Article
doi.org/10.1002/chem.202300318
Chemistry Europe
European Chemical Societies Publishing
www.chemeurj.org

A Predictive Model for the Pd-Catalyzed Site-Selective Oxidation of Diols

Nittert Marinus,[a] Niek N. H. M. Eisink,[a] Niels R. M. Reintjens,[a] Renger S. Dijkstra,[a] Remco W. A. Havenith,*[b, c] Adriaan J. Minnaard,*[a] and Martin D. Witte*[a]

Abstract: A predictive model, shaped as a set of rules, is presented that predicts site-selectivity in the mono-oxidation of diols by palladium-neocuproine catalysis. For this, the factors that govern this site-selectivity within diols and between different diols have been studied both experimentally and with computation. It is shown that an electronegative substituent antiperiplanar to the C–H bond retards hydride abstraction, resulting in a lower reactivity. This explains the selective oxidation of axial hydroxy groups in vicinal cis-diols. Furthermore, DFT calculations and competition experiments show how the reaction rate of different diols is determined by their configuration and conformational freedom. The model has been validated by the oxidation of several complex natural products, including two steroids. From a synthesis perspective, the model predicts whether a natural product comprising multiple hydroxy groups is a suitable substrate for site-selective palladium-catalyzed oxidation.

Introduction

The site-selective, late-stage functionalization of advanced synthetic intermediates and natural products has gained considerable attention in recent years.[1–3] This approach is often based on experimentally observed subtle reactivity differences within the substrate. However, when it comes to generalization of these site-selective functionalization methods, an in-depth understanding of the factors governing site-selectivity is crucial. These factors can be uncovered by careful determination of the site-selectivity of a reaction in a series of different substrates. This strategy has for example been used for the late stage functionalization of complex molecules by undirected C–H activation.[4–6] As more complex substrates can have multiple reactive sites, it is also essential to determine their relative reactivity, which can be done by intermolecular competition experiments with substrates containing a single reactive site.[7–10] The results of these studies are then translated into a reactivity scale or a predictive model that is more generally applicable and can predict the site-selectivity in unexplored substrates.

An example of a late-stage functionalization method is the site-selective oxidation of polyols with palladium neocuproine catalyst **1** (Figure 1). This catalyst, although original applied by the group of Waymouth for the oxidation of mono-ols, has proven to be particular efficient for the oxidation diols and polyols to the corresponding hydroxy ketones at room temperature with either oxygen or 1,4-benzoquinone (BQ) as the terminal oxidant.[11,12] Excellent site-selectivities are observed for various substrates.[13] In terminal 1,2-diols, the secondary hydroxy group is oxidized selectively over the primary hydroxy group (Scheme 1a–b).

Also the oxidation of internal 1,2-diols is often selective. The axial hydroxy group of conformationally restricted 1,2-*cis*-cyclohexane diols is oxidized preferentially (Scheme 1c).[13] In monosaccharides, oxidation takes place predominantly, if not solely, at the C3-position, which is the carbon atom furthest away from the endocyclic oxygen (Scheme 1d–e).[14–17] Interestingly, this site-selectivity is independent of the substitution pattern (e.g., glucose, galactose, mannose or rhamnose). Even

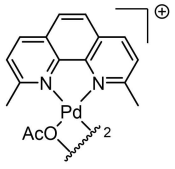

1

Figure 1. Palladium neocuproine catalyst **1**.

[a] N. Marinus, N. N. H. M. Eisink, N. R. M. Reintjens, R. S. Dijkstra, Prof. Dr. A. J. Minnaard, Prof. Dr. M. D. Witte
Stratingh Institute for Chemistry
University of Groningen
Nijenborgh 7, 9747 AG, Groningen (the Netherlands)
E-mail: m.d.witte@rug.nl
a.j.minnaard@rug.nl

[b] Prof. Dr. R. W. A. Havenith
Zernike Institute for Advanced Materials
University of Groningen
Nijenborgh 4, 9747 AG, Groningen (the Netherlands)

[c] Prof. Dr. R. W. A. Havenith
Ghent Quantum Chemistry Group, Department of Chemistry
Ghent University
Krijgslaan 281 (S3), B-9000 Ghent (Belgium)
E-mail: r.w.a.havenith@rug.nl

Supporting information for this article is available on the WWW under https://doi.org/10.1002/chem.202300318

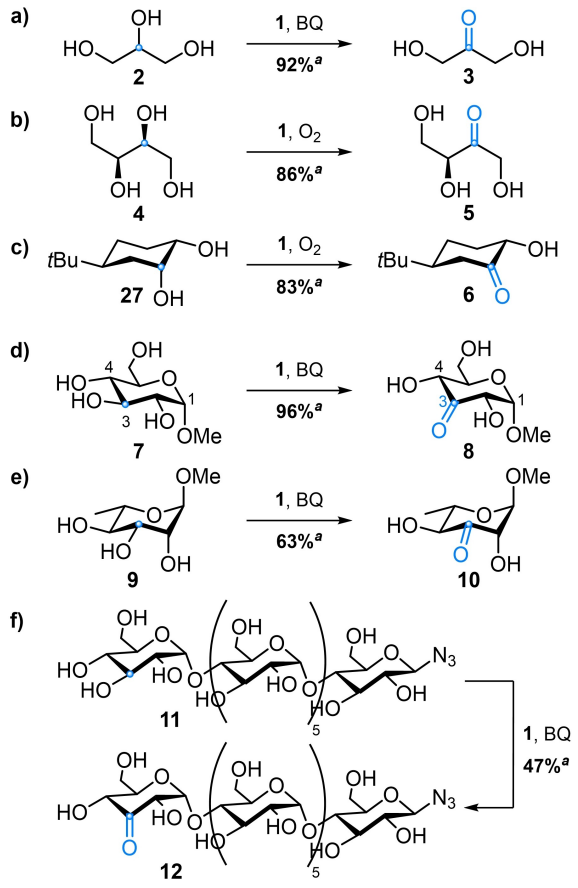

Scheme 1. Reported site-selective oxidation of diols by Pd-neocuproine catalyst **1**. Blue spheres represent the preferred oxidation site. a) & b) Examples that demonstrate the selectivity for secondary alcohols in vicinal diols. c) Example of preferential oxidation of the axial OH in a vicinal diol. d) & e) Examples that demonstrate the preferential oxidation of C3-OH in glycosides. f) Example of the site-selective oxidation in oligosaccharides, illustrating how sterics affect the site-selectivity. [a] Isolated yields.

when the substrate contains a *cis*-diol motif (i.e. axial C2–OH or C4–OH), the equatorial C3-hydroxy group is oxidized instead of the axial C2 or C4-hydroxy group (Scheme 1e). In oligomaltosides, polyols *par excellence*, oxidation is site-selective for the terminal glucose residue at the non-reducing end (Scheme 1f).[18]

Part of the site-selectivity observed for palladium neocuproine catalyst **1** can be explained by steric and stereoelectronic factors. A computational study by Wan et al. revealed that the ring oxygen lies at the basis of the C3-selectivity in pyranosides. The ring oxygen polarizes C1 and C5 by inductive electron density withdrawal, thereby also disfavoring buildup of positive charge at the neighboring C2 and C4. This renders C3 the most favored site for oxidation,[19] despite the fact that 1,3-diaxial interactions impose steric hindrance on the C3–H. Recent work by the group of Waymouth revealed that the stereo-electronic factors that favor C3–OH oxidation can be overcome with sterically hindered ligands, leading to catalysts that have a reduced C3-selectivity.[20] The selective oxidation of oligomaltosides can be explained by sterics, as the glucose residue at the non-reducing end is the most accessible.[21]

The results of these prior studies form an excellent starting point for the development of a model that predicts the site-selectivity of this catalytic oxidation. However, there are several questions that need to be addressed before a reliable model can be established. The selective oxidation of the axial hydroxy group in a cyclohexane 1,2-*cis*-diol is incongruent with the observation that the oxidation of pyranosides is C3-selective regardless of the stereochemistry of the hydroxy groups at C2, C3, and C4. Moreover, to be able to predict site-selectivity in complex substrates containing multiple diol motifs, the *relative* reactivity of the diols with similar electronic properties and steric hindrance needs to be determined.

In this study, we address these questions and formulate a reactivity model to predict the site-selectivity of the palladium-catalyzed oxidation reaction. The model is validated as well by subjecting a set of natural products with vicinal diols to the reaction.

Results and Discussion

We first focused our attention on factors that determine the site-selectivity within a diol in order to explain the apparent selectivity differences between 1,2-*cis*-diols in cyclohexanes (Scheme 1c) and in glycosides (Scheme 1d,e). Structural analysis of the 1,2-*cis*-cyclohexanediol **27** revealed that the α-hydrogen of the equatorial hydroxyl group is antiperiplanar to a C–H and to the neighboring axial hydroxyl group (indicated with the red arrow in Figure 2a). The α-hydrogen of the axial hydroxyl group is antiperiplanar to the C–C bonds of the cyclohexane and is synclinal to the equatorial alcohol (indicated with the green arrow in Figure 2a). We hypothesized that the observed selectivity for the axial OH resulted from this stereochemical difference. During hydride abstraction by the Pd catalyst (also referred to as β-H elimination in the catalytic cycle of **1**[12]), cationic character builds up on the carbon atom of the alcohol that is being oxidized. Vicinal electron-donating groups lower

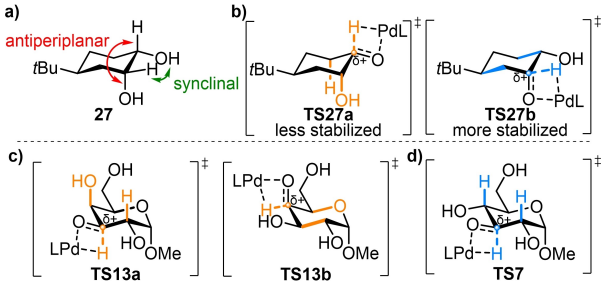

Figure 2. Hyperconjugative interactions in 1,2-*cis*-diols. a) the stereochemical relation between the α-hydrogen of the hydroxyl group that is being oxidized and the neighboring OH. b) The transition states that lead to oxidation of the equatorial and the axial OH. c,d) Transition states in c) galactosides and d) glucosides. Transition states that have hyperconjugative interactions with vicinal electronegative substituents are depicted in orange. Transition states that have solely hyperconjugative interactions with C–C or C–H are depicted in blue.

the energy-barrier for Pd-catalyzed oxidation of alcohols (i.e. activate the substrate),[22] as they stabilize the developing positive charge in the transition state (TS) via hyperconjugative interactions. Electronegative substituents, irrespective whether they are synclinal or antiperiplanar to the hydroxyl group that is being oxidized, should deactivate the substrate, as the electronegative substituents destabilize the TS by inductive withdrawal of electron density. However, from the results with **27**, we concluded that a vicinal antiperiplanar electronegative substituent has a stronger deactivating effect, than a synclinal substituent. We hypothesized that the σ_{C-X} orbital stabilizes the TS of hydride abstraction less efficiently via hyperconjugation, since a σ_{C-X} orbital is a relative poor electron density donor, compared to σ_{C-H} or σ_{C-C} orbitals.[23,24] Consequently, an antiperiplanar electronegative substituent should increase the activation energy and reduce the reactivity of the vicinal C–H bond. Along this line of reasoning, oxidation of the equatorial hydroxyl group in compound **27** is disfavored, as the TS of hydride abstraction (**TS27a**) is stabilized by one antiperiplanar C–H and by the poorly donating antiperiplanar C–OH (Figure 2b, orange bonds). Whereas the TS of hydride abstraction at the carbon of the axial hydroxyl (**TS27b**) is stabilized relatively more, i.e., by two C–C bonds (Figure 2b, blue bonds).

The results on glycosides with an axial hydroxy group at the C2/C4-position (Scheme 1e) are also in line with the above formulated hypothesis, which at first sight may not be obvious. The axial hydroxy group at the C2/C4-position is antiperiplanar to the vicinal C3–H (exemplified in Figure 2c for galactoside **TS13a**, orange bonds), thereby deactivating the C3 for oxidation. From the 1,2-*cis*-diols in cyclohexanes, oxidation of the axial hydroxyl group would be expected. However, in the case of a glycoside, hydride abstraction of the C2/C4 position should also be disfavored, since the C–H bond is antiperiplanar to the endocyclic oxygen (Figure 2c, orange bonds for galactoside in **TS13b**). The inductive electron withdrawing effect of the ring oxygen means that the C3 position is still the preferred oxidation site. The axial hydroxy group at the C2/C4-position makes that these glycosides are deactivated, compared to glucosides.[17] This was corroborated by an oxidative competition experiment between methyl α-galactoside **13** and methyl α-glucoside **7**. An approximate twofold larger oxidation rate was observed for methyl α-glucoside **7** (see below, Figure 3c) because the C3-hydrogen of glucoside **7** is not antiperiplanar to an electronegative substituent (Figure 2d, blue bonds).

To validate the hypothesis that electronegative substituents retard hydride abstraction of antiperiplanar C–H bonds, 4-deoxy-4-fluoro-glucoside **14** and 4-deoxy-4-fluoro-galactoside **16** were oxidized by the palladium neocuproine catalyst (**1**) and 1,4-benzoquinone (BQ) (Scheme 2). Both substrates have a C2–C3 *trans*-diequatorial diol that can chelate with the Pd

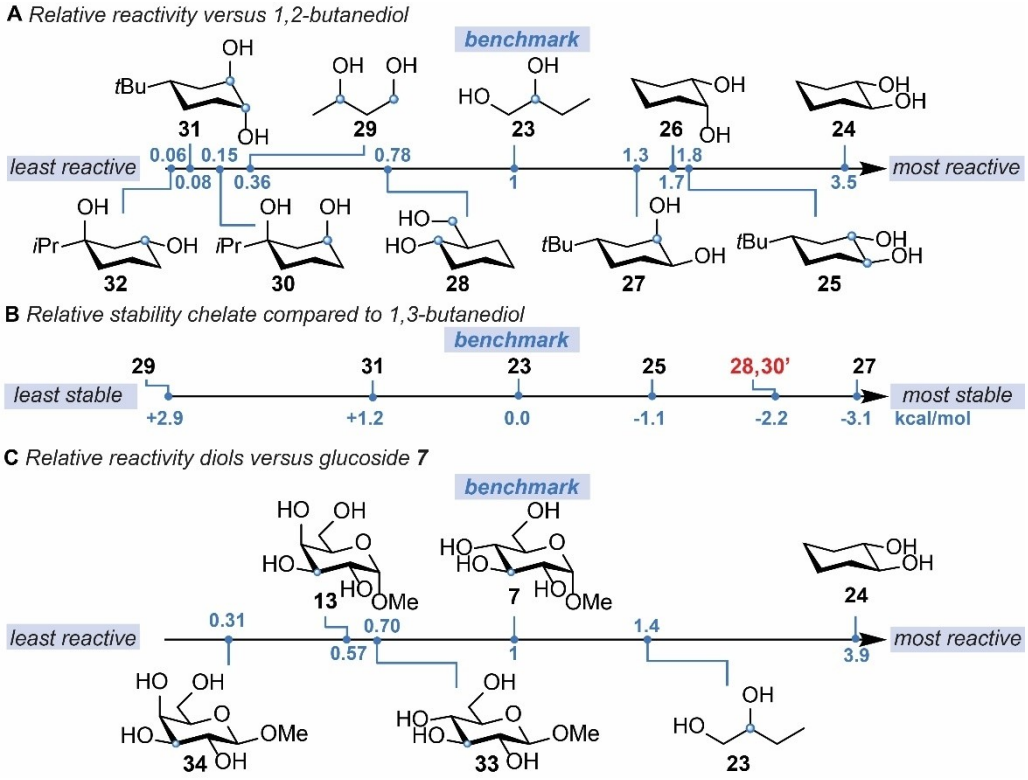

Figure 3. Relative reactivity of diols **23–34**. (a) Relative reactivity compared to 1,2-butanediol **23**. Conditions: 1 equiv. benchmark diol **23**, 1 equiv. competitor diol, 3 mol% **1** and 1 equiv. BQ in DMSO-*d6*. (b) The computed relative stability of the palladium-substrate complexes compared to benchmark diol **23**. 1,3-Diols **28** and **30'**, labeled in red, form a stable complex, but show low reactivity. (c) Relative reactivity of diols and glycosides compared to glucoside **7**. Conditions: 1 equiv. benchmark **7**, 1 equiv. competitor, 3 mol% **1** and 1 equiv. BQ in DMSO-*d6*. Blue spheres in the substrate indicate the preferred oxidation site. Relative reactivity was calculated by dividing conversion of competitor diol by conversion of benchmark diol. The relative reactivity is based on the average of two experiments.

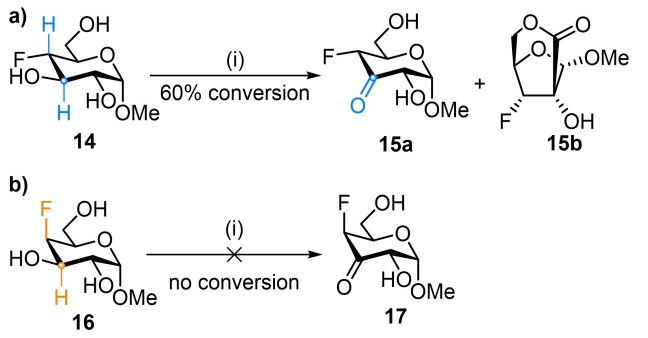

Scheme 2. Oxidation of 4-deoxy-4-fluoro-glycosides. i) 2.5 mol% **1**, 1 equiv. BQ in DMSO-*d6*. Product ratio **15a**/**15b**: 1/1; Depicted in blue and orange are respectively the σ_{C-H} and σ_{C-X} bonds at the C4 that have hyperconjugative interactions with the C3–H that is being abstracted.

catalyst, and a fluoro substituent at C4 that is either in the equatorial or the axial position. *Gluco*-configured substrate **14** should oxidize faster than *galacto*-configured **16** if hyperconjugative interactions play a role.

Oxidation of 4-deoxy-4-fluoro-glucoside **14** proceeded slowly compared to our benchmark methyl α-glucoside **7** (Scheme 2a). Clearly, the through-bond inductive effect of the fluoride deactivates the substrate significantly. Nevertheless, overnight reaction resulted in 60% conversion of **14**, of which 30% was 3-keto-glucose **15a**. The remaining 30% was rearranged product **15b** resulting from overoxidation of **15a** (SI: Figure S1). Thereafter, 4-deoxy-4-fluoro-galactoside **16** was subjected to the same conditions (Scheme 2b). Whereas *gluco*-configured substrate **14** was amenable to oxidation, *galacto*-configured **16** carrying an axial fluoride did not show any conversion and remained therefore inert towards oxidation. These results underline the importance of the antiperiplanar configuration of electronegative substituents.[25]

To validate our hypotheses further, C3-branched glycosides **18** and **21** were subjected to the oxidation reaction (Scheme 3). Their non-branched parent compounds, glucoside **7** and methyl allopyranoside respectively, oxidize selectively at C3.[26] However, methyl branching at C3, which prevents oxidation at that position, should direct the oxidation to the C2 or C4-position. That is, if the substrates are still amenable to oxidation. Indeed, oxidation of 3-*C*-methyl-glucoside **18** under the standard conditions at room temperature resulted in a mixture of C4- and C2-oxidized products (**19**:**20**/7:3, respectively). The preference for the C4 over the C2 is also in line with the hypothesis, as the axial OMe at C1 deactivates the C2 position. In contrast, 3-*C*-methyl-alloside **21** oxidized slowly at room temperature (only 27% conversion after overnight reaction). Interestingly, oxidation of the primary C6–OH was observed and **22** was identified as the major product (Scheme 3b). Similar results were obtained with beta-3-*C*-methyl-alloside. This difference in the oxidation of **18** and **21** can now be explained by a difference in hyperconjugative interactions.

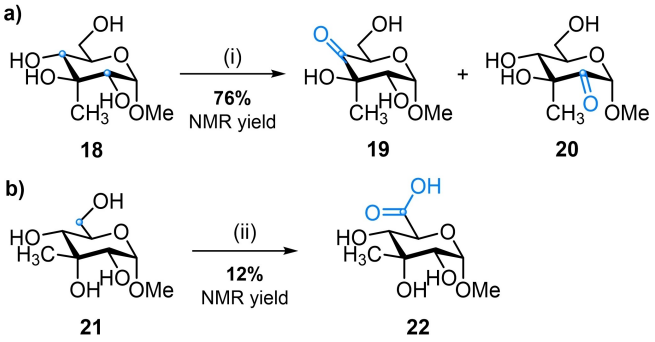

Scheme 3. Oxidation of 3-C-methyl-glycosides. i) 2.5 mol% **1**, 1 equiv. BQ in DMSO-d6, overnight at RT. Product ratio **19**/**20**: 7/3; ii) 2.5 mol% **1**, 2 equiv. BQ in DMSO-d6, overnight at RT gave **22** as the major product, conversion 27%, NMR yield 12%. Blue spheres in the substrate indicate the preferred oxidation site.

The combined deactivation of the C2- and C4-positions in **21** by the inductive effect of the ring oxygen, and the axial C3–OH, leaves only the primary C6–OH amenable for oxidation. These results corroborate the hypothesis that an antiperiplanar electronegative substituent retards the oxidation reaction. Attempts to determine if the deactivating effect by antiperiplanar electronegative substituents is more general were unsuccessful, since other oxidation methods either gave low conversions or oxidized the primary alcohol preferentially (Supporting Information Table S8).

Having investigated factors that govern the site-selectivity within a diol, we subsequently focused our attention on the reactivity between diols. Previous studies already demonstrated the importance of the stereo-electronic nature of the diol on its reactivity. Electronegative substituents as well as steric hindrance (see above) reduce the reactivity of the diol towards oxidation by palladium catalyst **1**. This allows to predict the preferential oxidation site in substrates that have two or more diol motifs that are very different in nature. Thus far, however, little is known about the selectivity in the palladium-catalyzed oxidation of diols that have a similar stereo-electronic nature. We reasoned that a qualitative reactivity scale of small diol substrates might provide this insight.

To obtain such a reactivity scale, the relative reactivity of ten structurally different diols was assessed in competition experiments. These ten substrates (1,2- and 1,3-diols **23**–**32**) possess different configurations and degrees of conformational freedom, but are stereo-electronically similar and suitable substrates for the oxidation with catalyst **1** (Supporting Information: page S62–S67). In the competition experiments, a benchmark diol, competitor diol and terminal oxidant BQ were mixed in a 1:1:1 ratio and oxidized with catalyst **1**. We selected these reaction conditions to determine the relative reactivity under synthetically relevant conditions. 1,2-Butanediol (**23**) and *trans*-1,2-cyclohexanediol (**24**) served as benchmark substrates. The relative reactivity was calculated by dividing the conversion of the competitor diol by the conversion of the benchmark substrate. A value higher than one indicates that the competitor diol is more reactive than the benchmark substrate, while a value lower than one indicates that the competitor diol is less reactive than the benchmark. Ranking of the different diols

yields a qualitative reactivity scale for the oxidation reaction (Figure 3a and S2, Table S9 and S10).

From Figure 3a, it is apparent that 1,2-cyclohexanediols that can adopt a *trans*-diequatorial conformation (**24** and **25**) are the most reactive substrates for the Pd-catalyzed oxidation reaction. *Trans*-1,2-cyclohexanediol (**24**) is 3.5 times more reactive than 1,2-butanediol (**23**). *Trans*-diol **25**, containing a *tert*-butyl substituent that restricts conformational freedom, is 1.8 times more reactive than **23**, but the reactivity of **24** and **25** is comparable when they are compared directly (Figure S2).

1,2-*cis*-cyclohexanediols **26** and **27** were the second most reactive substrates in the oxidation reaction. *Cis*-diol **26** had an approximately two-fold lower reactivity than *trans*-diol **24** (Figure 3a and S2). The two-fold reactivity difference between 1,2-*cis* and *trans*-diols is a recurring factor and also observed in competition experiments between the conformationally restricted *trans*-diol **25** and *cis*-diol **27** (relative reactivity of **27** vs. **25**: 0.58, Supporting Information: Table S14) and in competition experiments between monosaccharides (Supporting Information: Table S15).

The competition experiments showed that the acyclic 1,2-diol **23** is more reactive than 1,3-diols. In all cases, the conversions of the 1,3-diols were lower than that of the benchmark 1,2-diol **23** (Figure 3a). Especially relative to *trans*-1,2-cyclohexanediol (**24**), 1,3-diols were poor substrates, exhibiting at least five-fold lower reactivity (Figure S2).

Diols **30**, **31** and **32** revealed to be the least reactive diols. Only small amounts of oxidation products were formed in the competition experiment with 1,2-butanediol (**23**) (Figure 3a) and no oxidation of **30**–**32** at all was observed in the presence of *trans*-1,2-cyclohexanediol (**24**) (Figure S2). The reactivity trend observed in Figure 3a was confirmed when the competition experiments were performed in CD_3CN instead of DMSO-*d6*. The relative reactivities in CD_3CN were overall slightly closer to one. Erosion of relativity reactivity in CD_3CN resulted, at least, in part from over-oxidation by competing aerobic Pd-catalyzed oxidation (Supporting Information: Table S13). This result suggests that bigger relative reactivity differences maybe obtained when using sub-stoichiometric BQ and experiments with 0.2 equivalents of BQ confirmed this (Supporting Information: Table S11). However, lowering the BQ loading is from a synthetic point of view not beneficial.

A partial explanation for the observed differences in reactivity can be found in the suitability of these diols to chelate to the palladium catalyst. Earlier work by Waymouth and co-workers already showed the importance of chelation in the Pd catalyzed oxidation.[13] Their mechanistic studies revealed that vicinal diols react considerably faster than mono-ols, because these substrates rapidly form a hydroxyalkoxide chelate with the Pd-catalyst. As a result, hydride abstraction becomes the rate-determining step in the oxidation of 1,2-diols, rather than complexation to the catalyst, which is the rate-determining step for mono-ols. To further elucidate the role of the chelation efficiency on the relative reactivity, the stability of the various hydroxyalkoxide complexes was calculated with DFT (Supporting Information: Figure S3 and S4). The computed stabilities of the complexes largely follow the trends observed in the reactivity scale, except for 1,3-diol **28** and di-axial 1,3-diol **30** (Figure 3a and b). The DFT calculations on the 1,3-trans-diol **32′**, which resembles diol **32** but contains a *tert*-butyl group instead of a *iso*-propyl group, did not converge to a stable hydroxyalkoxide complex. From this result, it can be concluded that 1,3-trans-diol **32** behaves like a mono-ol in the oxidation reaction and the low reactivity of **32** is in line with this. The hydroxyalkoxide complexes formed by acyclic 1,3-diol **29** and 1,2-*trans*-diaxial diol **31** were computed to be less stable than those formed by 1,2-diol **23**. The lower stability of the hydroxyalkoxide complex of 1,2-*trans*-diaxial diol **31** can be attributed to the conformational change that the cyclohexane ring has undergone upon chelation to the catalyst. In the computed complex, diol **31** is in the energetically less favorable twist-boat conformation. The differences in stability between the hydroxyalkoxide complex of **29** and **23** resulted from an increase in the binding entropy as well as a decrease in the binding enthalpy. The lower stability of hydroxyalkoxide complexes **29** and **31** is reflected in the reactivity scale.

For diols **25**&**27**, which were found to be more reactive than **23**, the computed complexes were indeed more stable than that formed by acyclic 1,2-diol **23**.

Not all the relative reactivity difference can be explained by the differences in the stability of the hydroxyalkoxide complexes. Diol **28** and di-axial 1,3-diol **30′**, the latter resembles diol **30** but contains a *tert*-butyl group instead of a *iso*-propyl group, were computed to chelate well with palladium. The fact that both **28** and **30** showed relative poor reactivity in the competition experiments indicates that other factors, such as the activation energies for β-H elimination should not be disregarded. The reaction coordinates for the oxidation of the secondary hydroxy group in **23**, **28** and **29**, determined by DFT calculation,[27] confirmed this (Figure S6–S8). Compared to linear diols **23** and **29**, which have similar activation barriers, the activation energy for β-H elimination in **28** is considerably higher.

Altogether, these results indicated that the chelation efficiency should be taken in consideration in the predictive model, especially for substrates that form comparatively less stable hydroxyalkoxide complexes.

We were also interested to know what the relative reactivity of methyl α-glucoside **7** (our benchmark monosaccharide) would be, compared to 1,2-*trans*-cyclohexanediol **24**, 1,2-butanediol **23**, and other pyranosides (Figure 3c). A competition experiment showed that *trans*-diol **24** is approximately four times more reactive than glucoside **7**. The reactivity difference is not caused by chelation effects, since both substrates (**7**&**29**) contain only *trans*-diols. Instead, pyranosides oxidize inherently slower than cyclohexyl diols because of the polarizing ring oxygen (see above).[19] The competition experiment between α-glucoside **7** and 1,2-butanediol (**23**) showed that **7** was slightly less reactive than **23**. In the competition experiment between methyl α-glucopyranoside (**7**) and methyl α-galactopyranoside (**13**) a near twofold reactivity difference was observed. As expected, α-galactoside **13** was less reactive due to the deactivating effect of the axial C4 hydroxy group (see above). Interestingly, methyl β-glucopyranoside (**33**) showed a de-

creased reactivity as well. The combined effects of an axial C4 hydroxyl and a β-configuration culminates in a threefold decreased reactivity for methyl β-galactopyranoside (**34**) when competed against α-glucoside **7**.[17]

The relative reactivities in Figures 3a and 3c allow prediction of the preferential oxidation site in substrates that contain multiple diols, even when the diols are of similar stereoelectronic nature. To obtain a synthetically relevant selectivity, an approximate threefold reactivity difference (smaller than 0.33 or higher than 3) is considered desirable.

A closer inspection of the oxidation products obtained in the competition experiments revealed that all diols were suitable substrates for the oxidation reaction and that most oxidized selectively. However, conformational restricted *trans*-1,2-cyclohexanediols **25**&**31** and 1,3-diols **28**&**29** did not oxidize selectively. Oxidation of *trans*-diequatorial 1,2-cyclohexanediol **25** yielded hydroxyketone **6** (for structure see Scheme 1) and the corresponding regio isomer (for structure of **S20** see Supporting Information), which was the expected outcome. Interestingly, *trans*-diaxial 1,2-cyclohexanediol rapidly epimerized upon oxidation, and also gave a mixture of **6** and the corresponding regio isomer (see Supporting Information: **S20**). The results for 1,3-diols **28**&**29** surprised us. We expected that, as for 1,2-diols, formation of the hydroxyalkoxide complex should favor the oxidation of the secondary hydroxy group in 1,3-diols (Scheme 4a). Instead, oxidation of 1,3-butanediol did not proceed selectively and ketone **36** and aldehyde **37** were formed in a 1/1 ratio (Scheme 4b). Similarly, oxidation of 1,3-diol **28** resulted in a mixture of ketone **38** and aldehyde **39** (Scheme 4c).

In an attempt to explain these results, the reaction coordinates involving oxidation of primary hydroxyl group in **23**, **28** and **29** were determined by DTF-calculations (Figure S6–8).[27] The hydroxyalkoxide complexes of the diol and palladium were chosen as the reference point in the calculations. Previous DFT calculations by Chung et al. had already shown that β-H elimination (the product-determining step) from the secondary position in 1,2-propane diol is more favorable than from the primary position.[13] Similarly, our computed activation energy for β-H elimination in 1,2-butanediol (**23**) for the secondary alkoxide was considerably lower than that of the primary

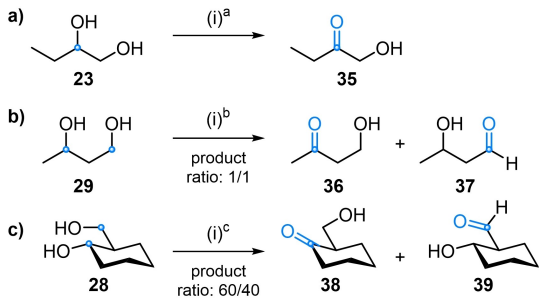

Scheme 4. Oxidation of 1,2- and 1,3-butanediol. i) 3 mol% **1** and 1 equiv. BQ in DMSO-*d6*; [a] full conversion, 100% selectivity; [b] 70% conversion, selectivity: 50%/50% (**36**/**37**); [c] 85% conversion, selectivity: 60%/40% (**38**/**39**).

alkoxide: $\Delta\Delta G^{\ddagger}_{1,2\text{-diol }\mathbf{23}} = 7.3$ kcal/mol (Chung et al. calculated a $\Delta\Delta G^{\ddagger}$ of 4.9 kcal/mol for 1,2-propanediol). The β-H elimination for the secondary alkoxide of 1,3-diol **29** and **28** was still favored over the primary one, but the differences between the barriers were smaller: $\Delta\Delta G^{\ddagger}_{1,3\text{-diol}}$ **29** = 2.7 kcal/mol and $\Delta\Delta G^{\ddagger}_{1,3\text{-diol}}$ **28** = 3.1 kcal/mol, respectively.

The results from these calculations are consistent with the selectivities observed experimentally in Scheme 4, but do not provide an explanation for the difference. Therefore, the Activation Strain Model[28] together with the Energy Decomposition Analysis[29] was applied on compounds **23**, **28** and **29** to shed light on the energy differences between the transitions states (Figure 4a). These calculations showed that the strain in the Pd fragment is comparable for all TS, and that the difference in relative strain originates from the strain in the organic fragment. In all cases, the TS for oxidation at the secondary alcohol are less strained than for the primary alcohol (i.e. energetically more favorable). Interestingly, the difference in relative strain for linear 1,3-diol **29** is comparably less than for diols **23** and **28**. The bonding energy between the fragments is substrate dependent, but is more favorable in the TS that leads to oxidation of the primary hydroxyl group. In 1,3-diols, the bonding energy between the fragments almost fully compensates the unfavorable strain in the organic fragment. A further break-down of the bonding energies in **28** revealed that primarily electrostatic interactions between the catalyst and the substrate contribute to the favorable bonding energy in the primary alcohol.

A further NBO analysis was performed on the organic fragment of transition states of **23** and **29** to understand the relatively small difference in strain in linear 1,3-diol **29**.[30,31] Removal of hyperconjugative interactions from strongly occupied NBOs (indicated in Figure 4b in blue/green) to the antibonding σ^*_{C-H} bond (indicated in yellow/red in Figure 4b) destabilized TS in all cases, but comparatively more for the secondary hydroxy group in 1,2-butanediol. The TS of the β-H elimination at the secondary alcohol in 1,2-butanediol was stabilized by two σ_{C-H} orbitals, whereas in 1,3-butanediol it was stabilized by one σ_{C-H} and one σ_{C-C} orbital. In our analyses and according to literature, σ_{C-H} bonds are better donors than σ_{C-C} orbitals,[23,32] hence the TS of β-H elimination at the secondary alcohol in 1,3-butanediol is less stabilized compared to the TS in 1,2-butanediol. In conclusion, these results show that in 1,3-diols the lack of stabilization in the TS can be compensated by favorable bonding interactions.

Based on the results herein and the previously published work by Waymouth and our group, the following model was formulated. The list of rules helps to predict the preferential site of oxidation within a polyol and also gives an estimation of the relative reactivities between diols:

Selectivity within a diol/polyol:

1. In terminal 1,2-diols, the secondary alcohol is oxidized selectively over the primary alcohol; terminal 1,3-diols do not oxidize selectively.
2. In internal 1,2-diols (and polyols), the most activated hydroxy group is oxidized. Hydroxy groups can be deactivated by:

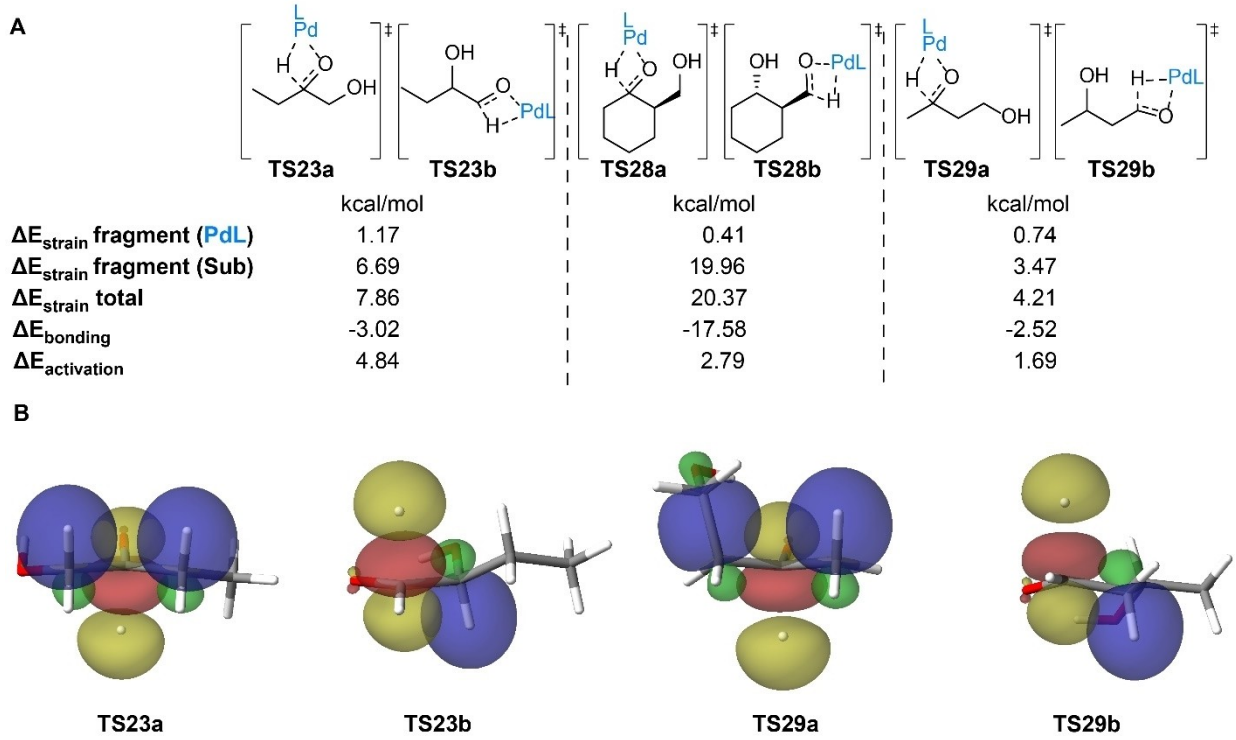

Figure 4. Computational study to determine the differences in site-selectivity in 1,2 and 1,3-diols. (a) Activation Strain Model together with the Energy Decomposition Analysis were performed to determine the relative difference in strain. The TS was divided in the Palladium fragment (colored blue) and the substrate fragment (colored black). The depicted relative strain and bonding energies are the difference in energy between the fragment leading to oxidation of the primary position and the fragment leading to oxidation of the secondary position. (b) Interactions between the strongly occupied NBOs (blue/green) and the σ*C–H bond (yellow/red) that were deleted from the Fock matrix.

a. An electronegative substituent antiperiplanar to a C–H bond. Notable example: in vicinal *cis*-cyclohexanediols the axial hydroxy group is preferably oxidized.
b. Inductive effects. Notable example: In pyranosides the hydroxy group that is furthest away from the endocyclic ring oxygen is preferably oxidized (C3-position). The site-selectivity in pyranosides is independent of its configuration.

Selectivity between diols:

3. In substrates that have diols that are electronically different, the most activated diol will be oxidized.
a. Inductive effects reduce the reactivity. Pyranosides oxidize inherently slower than hydrocarbon diols because of the polarizing ring oxygen. For example: α-glucopyranoside is four times less reactive than a cyclic 1,2-*trans*-di-equatorial-diol (Figure 3c).
b. Electronegative substituents antiperiplanar to oxidation sites retard the oxidation. For example: α-galactopyranoside **13** is approximately twofold less reactive than α-glucopyranoside **7**, due to an axial C4 hydroxy group (Figure 3c).
c. In pyranosides: β-pyranosides have a lower reactivity than α-pyranosides.
4. In substrates that have diols that are electronically comparable, diols that chelate most readily to the catalyst oxidizes the fastest. Chelation efficiency is determined by:
a. Steric hindrance. More accessible diols oxidize faster. For example: in oligomaltoses the C3-OH at the non-reducing end is preferentially oxidized, as the other C3-positions are less accessible for the catalyst.
b. Configuration and degrees of conformational freedom. The relative reactivities of different diols have the following order: cyclic 1,2-*trans*-di-equatorial-diol > cyclic 1,2-*cis*-diol > acyclic 1,2-diol > partially cyclic and acyclic 1,3-diol > acyclic 1,3-diol > cyclic 1,2-*trans*-diaxial-diol ≈ cyclic 1,3-diaxial-diol ≈ cyclic 1,3-*trans*-diol (Figure 3a).

The predictive value of the model described above was evaluated by the oxidation of several complex substrates that contain multiple vicinal diols. First, we applied the model to predict the site-selectivity of the oxidation of methyl α-melibiose (**40**). This disaccharide consists of a galactose residue that is linked to a glucose residue via an α-(1-6)-linkage (Scheme 5a). Both sugar residues should oxidize at the C3–OH due to the inductive effect of the ring oxygen. In addition, according to the model, the axial C4–OH in the galactose residue retards oxidation of the neighboring C3-position. Oxidation should therefore preferentially occur at the glucose residue and should yield preferentially 3-ketomelibiose **41**. This was confirmed experimentally by performing the oxidation of **40** on small scale in DMSO-*d6*. Analysis of the reaction mixture by ^{1}H NMR showed that 75% of the input material had been oxidized after 28 h. The major product of the reaction was the expected 3-keto-meliobiose **41** (47% NMR yield), which was formed together with some unidentified (over)oxidation prod-

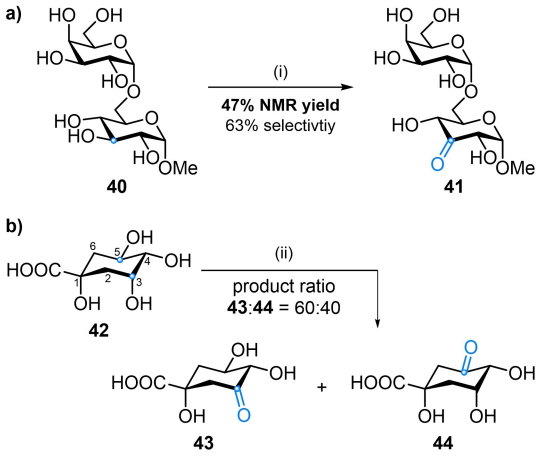

Scheme 5. Oxidation of methyl α-melibiose and quinic acid. i) 17 mol% **1**, 1 equiv. BQ in DMSO-*d6*. 75% conversion. Selectivity calculated by dividing the NMR yield by conversion; ii) 2.5 mol% **1**, 1 equiv. BQ in DMSO-*d6*. 71% conversion.

ucts. The product selectivity was determined by dividing the yield of **41** by the total conversion of **40**. A product selectivity of 63% was obtained, which closely matches with the relative reactivity between glucoside **7** and galactoside **13** (Figure 3c). Ketone **41** was isolated in 38% yield.[27]

Next, we applied the model to predict the site-selectivity in the oxidation of quinic acid (**42**) (Scheme 5b).[33–35] This polyol contains three secondary hydroxy groups that have a *cis* and a *trans* relation, as well as a tertiary alcohol. According to our model, the C4–OH in quinic acid (see Scheme 5b for numbering) is deactivated because of the vicinal axial C3–OH. The model predicts that both the hydroxy group at the C3- and the C5-position would be prone to oxidation, with a slight preference for the C5–OH because it is part of a *trans*-1,2-diequatorial diol. However, according to our reactivity scale (Figure 3a), 1,3-diaxial diols can be oxidized, albeit slowly. Since two chelation modes, namely chelation to the *cis*-1,2-diol and to the 1,3-diaxial diol can contribute to oxidation of the C3–OH, while only one chelation mode contributes to C5–OH oxidation, we anticipated that the preference for the C5–OH would be reduced. Indeed, oxidation of **42** resulted primarily in the expected C3- and the C5-keto products. NMR showed that the oxidation reaction had a slight preference for the C3–OH over the C5–OH. This marginal difference confirms that the regioselectivity follows from the sum of the chelation modes. This reasoning is further supported by the site-selectivities observed in the oxidation of carba-sugars.[19]

To verify whether the model can predict selectivity between two isolated vicinal diols, the steroids *epi*-brassinolide (**45**) and *epi*-castasterone (**46**) were oxidized (Figure 5a). Both steroids contain a cyclic *cis*-diol and an acyclic vicinal diol. For the selectivity within the diols, the model predicts that (1) in the *cis*-1,2-diol the axial hydroxy group at C3 is oxidized preferentially over the equatorial alcohol at C2 and (2) the most accessible hydroxy group in the acyclic diol is preferentially oxidized. Analysis of potential conformations (Figure 5b and Figure 5c)

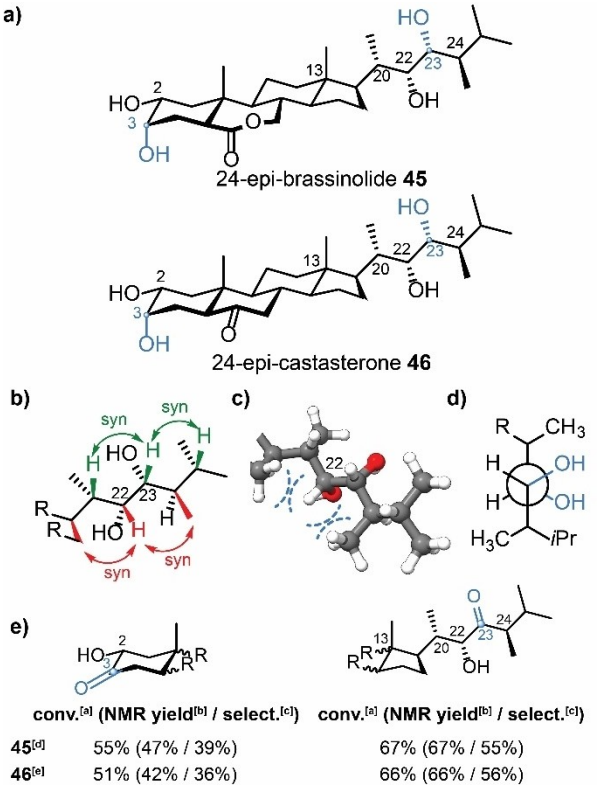

Figure 5. (a) Structures of the steroids *epi*-brassinolide (**45**) and *epi*-castasterone (**46**) and the preferred oxidation site in blue. (b,c) Conformational analysis of the steric hindrance at C22 (syn relation indicated with red arrows) and C23 (syn relation indicated with the green arrows). Picture in c was rendered with Chem3D and processed with ChimeraX.[36] (d) Newman projection of the side chain of **45** and **46**. (e) Oxidation of steroids. [a] Conversion of the isolated diol motif. [b] NMR yield of the depicted diol. [c] Selectivities for each alcohol were calculated by dividing the NMR yield by the combined conversion of the diol motifs. [d] 2.5 mol% **1**, 1.2 equiv. BQ in DMSO-*d6*. [e] 2.5 mol% **1**, 1.25 equiv. BQ in DMSO-*d6*.

showed that the H-atom at C23 is the most accessible. The C23 can adopt a presumed conformation in which the C–H is *syn* to the C–H at C21 and C25. In the depicted conformation, there is considerable more steric hindrance around the H-atom at C22. This atom has a 1,3-*syn* relationship to both the C–C of the cyclopentane ring and the methyl substituent at C24. Also in other conformations, the H-atom at C23 is the most accessible (Figure S9). The methyl substituent at C13 presumably prevents the side chain from adopting a more suitable conformation.

For the selectivity between the diols, the model predicts preferential oxidation of the cyclic *cis*-diol over the acyclic diol. However, we expected the differences in selectivity to be minimal, in particular also because the acyclic diols in these substrates likely have considerably less degrees of freedom, compared to 1,2-butanediol. The bulky groups of the side chains will predominantly adopt an antiperiplanar orientation to minimize steric interactions. As a result, the hydroxy groups will be *gauche* to each other (see Newman projection in Figure 5d). This conformation mimics the most favorable motif, i.e. a 1,2-*trans*-di-equatorial-diol, for chelation to the catalyst and may enhance the oxidation of the acyclic diol. Oxidation of

45–**46** was performed and monitored by NMR. Starting material, mono-, double, and even triple (over)oxidation products were observed. The selectivity for the respective site was determined by dividing the NMR yield by the total conversion (Figure 5e).

The selectivities within the vicinal diols are correctly predicted. The sterically least hindered hydroxy groups are oxidized preferentially in the case of the acyclic diols, and the axial hydroxy groups were preferably oxidized over the equatorial alcohols in **45** and **46**. Taking the conformational analysis into account, the model also predicts the selectivities between the diols correctly, since the "trans-di-equatorial-like" acyclic diol is preferentially oxidized over the cis diol.

Overall, the validation studies underline the predictive value of our model. In particular, the site-selectivity within an isolated diol can be predicted with reasonable confidence. The developed relative reactivity scale can also be used to reliably estimate the preferential oxidation site in substrates that contain multiple diols, even when the reactivity differences of the diols are minimal. However, not only the type of chelation (trans versus cis versus 1,3-diaxial), but also the number of possible chelation modes that leads to a product should be taken into account, and a careful conformational analysis is needed.

Conclusions

In conclusion, a set of rules has been formulated that predicts the site-selectivity of the palladium-neocuproine catalyzed alcohol oxidation within diols, between diols, and in pyranosides. An electronegative substituent antiperiplanar to a C–H bond retards hydride abstraction of that C–H bond and therefore displays a lower reactivity. For that reason, the oxidation rate of an equatorial hydroxy group is lower when part of a vicinal cis-diol. Furthermore, we have shown that the relative oxidation rates between diols are influenced by their configuration and conformational freedom. With the model, the oxidation selectivity within a diol and between diols can be predicted, as was shown for the disaccharide melibiose, quinic acid, and two steroids. From a synthesis perspective, our model can estimate whether a complex natural product could be a suitable substrate for site-selective oxidation with the Pd-catalyst. Substrates with diol motifs that have, according to the model, a threefold or higher reactivity difference can be oxidized with a reasonable degree of confidence to give synthetically relevant yields. We expect that our model will be useful as a prediction tool for future applications of the palladium catalyzed site-selective oxidation of diols.

Experimental Section

Oxidation of methyl 4-deoxy-4-fluoro-α-D–glucopyranoside (14): 4-Deoxy-4-fluoro glucoside **14** (23.5 mg 0.12 mmol, 1 equiv.) and 1,4-benzoquinone (13 mg, 0.12 mmol, 1 equiv.) were dissolved in DMSO-d_6 (400 μL, 0.3 M) and transferred to an NMR tube. A ^{1}H NMR spectrum was measured (d1 = 60) to determine the ratio of DMSO: starting material (DMSO was used as the internal standard). [(Neocuproine)PdOAc]$_2$OTf$_2$ (3 mg, 3 μmol, 2.5 mol%) was added to the NMR tube and the solution was mixed. After 3 h at room temperature the mixture was analyzed by NMR (d1 = 60) to determine the selectivity and to characterize the products by ^{1}H- and ^{13}C NMR. Analysis showed 33% conversion of **14** and products **15a** (NMR yield 23%, selectivity 70%) and **15b** (NMR yield 10%, selectivity 30%) in a ratio of 7/3, respectively. Analysis after 16 h showed 60% conversion of **14** and products **15a** (NMR yield 30%, selectivity 50%) and **15b** (NMR yield 30%, selectivity 50%) in a ratio of 1/1, respectively. Product **15b** is the result of overoxidation of **15a** followed by α-ketol rearrangement (Figure S1).[17]

Characterization of **15a**: ^{1}H NMR (400 MHz, DMSO-d_6) δ 5.16 (dd, J = 48.4, 10.0 Hz, 1H, H4), 5.00 (d, J = 2.9 Hz, 1H, H1), 4.35 (d, J = 4.2 Hz, 1H, H2), 3.75–3.47 (m, 3H, H5 & H6), 3.30 (s, 3H, OCH_3); ^{13}C NMR (101 MHz, DMSO-d_6) δ 201.2 (d, J = 12.5 Hz, C3), 102.0 (C1), 87.6 (d, $J_{C,F}$ = 165.7 Hz, H4), 74.8 (C2), 72.3 (d, J = 23.5 Hz, C5), 59.8 (C6), 54.9 (OCH_3) Characterization of **15b**: ^{1}H NMR (400 MHz, DMSO-d_6) δ 5.21 (d, J = 54.0 Hz, H3), 4.86 (d, J = 12.0 Hz, 1H, H4), 4.79 (s, 1H, H1), 4.28 (d, J = 11.5 Hz, 1H, H5a), 4.16–4.11 (m, 1H, H5b), 3.36 (s, 3H, OCH_3); ^{13}C NMR (101 MHz, DMSO-d_6) δ 172.1 (C6), 102.7 (C1), 89.5 (d, J = 174.7 Hz, C3), 80.7 (d, J = 16.4 Hz, C2), 76.0 (d, J = 18.4 Hz, C4), 71.2 (d, J = 9.4 Hz, C5), 56.3 (OCH_3).

Oxidation of methyl 4-deoxy-4-fluoro-α-D–galactopyranoside (16): 4-Deoxy-4-fluorogalactoside (23.5 mg 0.12 mmol, 1 equiv.) and 1,4-benzoquinone (13 mg, 0.12 mmol, 1 equiv.) were dissolved in DMSO-d_6 (400 μL, 0.3 M) and transferred to an NMR tube. A ^{1}H NMR spectrum was measured (d1 = 60) to determine the ratio of DMSO: starting material (DMSO was used as the internal standard). [(Neocuproine)PdOAc]$_2$OTf$_2$ (3 mg, 3 μmol, 2.5 mol%) was added to the NMR tube and the solution was mixed. After 5 h at room temperature the mixture was analyzed by NMR (d1 = 60) to determine the selectivity and to characterize the products by ^{1}H- and ^{13}C NMR. Analysis: No or very little conversion was observed.

Oxidation of methyl 3-*C*-methyl-α-D–glucopyranoside (18): Glucoside **18** (4.5 mg, 22 μmol, 1 equiv.) and 1,4-benzoquinone (3.0 mg, 28 μmol, 1.3 equiv.) were dissolved in DMSO-d_6 (600 μL, 0.04 M) and transferred to an NMR tube. A ^{1}H NMR spectrum was measured (d1 = 60) to determine the ratio of DMSO:starting material (DMSO was used as the internal standard). [(Neocuproine)PdOAc]$_2$OTf$_2$ (1.2 mg, 1 μmol, 5.3 mol%) was added to the NMR tube and the solution was mixed. After 20 h at room temperature the starting material was fully converted and the mixture was analyzed by NMR by ^{1}H- and ^{13}C NMR (d1 = 60). Analysis showed full conversion of **18**. Products **19** (NMR yield 53%, selectivity 53%) and 20 (NMR yield 23%, selectivity 23%) were found in a ratio of 7/3, respectively (combined NMR yield of 76%). Characterization of **19**: ^{1}H NMR (600 MHz, DMSO-d_6) δ 4.95 (d, J = 4.3 Hz, 1H, H1), 4.38 (dd, J = 6.4, 4.7 Hz, 1H, H5), 4.00 (d, J = 4.3 Hz, 1H, H2), 3.48 (dd, J = 11.5, 4.6 Hz, 1H, H6a), 3.43 (dd, J = 11.5, 6.4 Hz, 1H, H6b), 3.34 (s, 3H, OCH_3), 2.19 (s, 3H, CH_3); ^{13}C NMR (151 MHz, DMSO-d_6) δ 206.9 (C4), 102.7 (C1), 86.2 (C3), 80.1 (C2 + C5), 59.7 (C6), 55.2 (OCH_3), 26.8 (CH_3). Characterization of 20: ^{1}H NMR (600 MHz, DMSO-d_6) δ 4.76 (s, 1H, H1), 4.12–4.05 (m, 1H, H5), 4.03 (d, J = 7.6 Hz, 1H, H4), 3.59 (dd, J = 11.9, 2.9 Hz, 1H, H6a), 3.43 (dd, J = 11.5, 6.4 Hz, 1H, H6b), 3.27 (s, 3H, OCH_3), 2.23 (s, 3H, CH_3); ^{13}C NMR (151 MHz, DMSO-d_6) δ 206.0 (C2), 109.4 (C1), 87.8 (C3), 83.9 (C5), 77.3 (C4), 61.1 (C6), 56.3 (OCH_3), 28.8 (CH_3).

Oxidation of methyl 3-*C*-methyl-α-D–allopyranoside (21): Alloside **21** (11 mg, 53 μmol, 1 equiv.) and 1,4-benzoquinone (11.5 mg, 106 μmol, 2 equiv.) were dissolved in DMSO-d_6 (600 μL, 0.09 M) and transferred to an NMR tube with one drop of D_2O. A ^{1}H NMR spectrum was measured (d1 = 60) to determine the ratio of DMSO: starting material (DMSO was used as the internal standard). [(Neocuproine)PdOAc]$_2$OTf$_2$ (1.4 mg, 1 μmol, 2.5 mol%) was added

to the NMR tube and the solution was mixed. After overnight incubation, 25% conversion was observed at room temperature, with **22** being the major product (12% NMR yield). Next, the NMR tube was heated to 50 °C for 1 h. At this point the conversion increased to 51% according to 1H NMR (NMR yield of **22**: 23%, selectivity: 45%). The C4 oxidation product was also formed in 7%. The mixture was further heated after which it was analyzed by NMR by 1H- and 13 C NMR. Other minor products were visible, but could not be identified or characterized.C4 minor products were visible. Characterization of **22**: ^{1}H NMR (400 MHz, DMSO-d_6) 4.57 (d, J= 4.0 Hz, 1H, H1), 3.99 (d, J=9.9 Hz, 1H, H5), 3.31-3.28 (m, 4H, H4, OCH3), 3.27 (d, J=4.8 Hz, 1H, H2), 1.13 (s, 3H). ^{13}C NMR (151 MHz, DMSO-d_6) δ 171.5 (C6), 100.2 (C1), 73.5 (C3), 72.0 (C4), 70.8 (C2), 68.9 (C5), 55.6 (OCH_3), 22.0 (CH_3).

Oxidation of methyl α-melibiose (40): Methyl α-melibioside (40, 15 mg, 42 μmol, 1 equiv.), 1,4-benzoquinone (4.6 mg, 42 μmol, 1 equiv.) and internal calibrant benzene (3 μL, 38 μmol, 0.9 equiv.) were added to a NMR tube and dissolved in DMSO (0.5 mL) with one drop of D_2O. The NMR tube was shaken to a homogeneous mixture and a ^{1}H NMR was taken (t_0 measurement, d1=60) prior addition of the catalyst. Next, catalyst [(2,9-dimethyl-1,10-phenanthroline)Pd(μ-OAc)]$_2$(OTf)$_2$ (1, 7.5 mg, 7.1 μmol, 17 mol%) was added. After 28 h at room temperature the mixture was filtered over a syringe filter and placed in another NMR tube. A ^{1}H NMR was measured again (t_1 measurement, d1=60) and 75% conversion of the starting material was observed with methyl α-D-galactopyranosyl-(1→6)-α-D-*ribo*-hex-3-ulopyranoside (**41**) as the major product (47% NMR yield, selectivity 63%). Other products are likely the result of oxidation at the galactoside subunit and/or oxidation at both galactoside and glucoseide subunits. These products could not be identified or characterized. Characterization of **41**: ^{1}H NMR (600 MHz, DMSO-d_6) δ 4.95 (d, J=4.1 Hz, 1H, H1), 4.74 (d, J=3.4 Hz, 1H, H1′), 4.31 (d, J=4.2 Hz, 1H, H2), 4.16 (d, J=9.7 Hz, 1H, H4), 3.79 (dd, J=11.7, 6.0 Hz, 1H, H6a), 3.73–3.48 (m, 7H), 3.46–3.41 (m, 1H, H6′b), 3.27 (s, 3H, OCH_3). ^{13}C NMR (151 MHz, DMSO-d_6) δ 205.8 (C3), 102.0 (C1), 98.9 (C1′), 74.5 (C2), 73.6, 72.0 (C4), 71.1, 69.3, 68.7, 68.3, 66.2 (C6), 60.4 (C6′), 54.5 (OCH_3).

Isolation of methyl α-D–galactopyranosyl-(1→6)-α-D–*ribo*-hex-3-ulopyranoside (41): Methyl α-melibioside (**40**, 43 mg, 0.12 mmol, 1 equiv.) and 1,4-benzoquinone (13 mg, 0.12 mmol, 1 equiv.) were dissolved in DMSO (0.8 mL). [(2,9-dimethyl-1,10-phenanthroline)Pd-(μ-OAc)]$_2$(OTf)$_2$ (1, 6 mg, 6 μmol, 5 mol%) was added and after 1 h at room temperature an additional amount of catalyst (1, 3 mg, 3 μmol, 2.5 mol%) was added. After 1.5 h the reaction was finished and the mixture was diluted with excess H_2O. The aqueous solution was freeze-dried and then purified by automated column chromatography (8 g silica column, MeOH/DCM gradient: 1:9→2:8). The product methyl α-D-galactopyranosyl-(1→6)-α-D-*ribo*-hex-3-ulopyranoside (**41**, 16.6 mg, isolated yield 38%) was obtained as a light brown solid. ^{1}H NMR (400 MHz, CD_3OD) δ 5.05 (d, J=4.2 Hz, 1H, H1), 4.97 (d, J=3.1 Hz, 1H, H1′), 4.45 (d, J=3.2 Hz, 1H, H2), 4.37 (d, J=9.9 Hz, 1H, H4), 4.02 (dd, J=11.6, 4.8 Hz, 1H, H6a), 3.94–3.89 (m, 2H, H5′+H3′), 3.87–3.75 (m, 4H, H2′+H4′+H5+H6b), 3.74–3.68 (m, 2H, H6′), 3.41 (s, 3H, OCH_3); ^{13}C NMR (400 MHz, CD_3OD) δ 206.9 (C3), 103.7 (C1), 100.4 (C1′), 76.0 (C2), 75.3 (C5), 73.6 (C4), 72.4 (C2′), 71.5, 71.1, 70.3, (C-3′+C-4′+C-5′), 67.3 (C6), 62.7 (C6′), 55.8 (OCH_3); HRMS (ESI): calculated for $C_{13}H_{21}O_{11}$ ([M–H]$^-$): 353.109, found: 353.109.

Oxidation of D-(−)-quinic acid (42): Quinic acid (**42**, 10.2 mg, 0.053 mmol, 1 equiv.) and 1,4-benzoquinone (5.7 mg, 0.053 mmol, 1 equiv.) were dissolved in DMSO-d_6 (0.6 mL) and transferred to a NMR tube with a drop of D_2O. A ^{1}H NMR spectrum was measured (d1=60) to determine the ratio of DMSO:starting material (DMSO was used as the internal standard). [(2,9-dimethyl-1,10-phenanthroline)Pd(μ-OAc)]$_2$(OTf)$_2$ (1, 1.4 mg, 1.3 μmol, 2.5 mol%) was added and the tube was shaken to form a homogeneous mixture and was left at room temperature for 9 h. The mixture was analyzed by NMR (^{1}H NMR: d1=60) and showed 71% conversion of **42** and products 3-keto **43** (NMR yield 42%, selectivity 59%) and 5-keto **44** (NMR yield 28%, selectivity 39%) were formed in a ratio of 60/40, respectively. Characterization of product **43**: ^{1}H NMR (400 MHz, DMSO-d_6) δ 3.95 (dd, J=9.2, 1.0 Hz, 1H, H4), 3.67 (ddd, J=11.1, 9.2, 5.1 Hz, 1H, H5), 2.92 (d, J=20.1 Hz, 1H, H2a), 2.36–2.27 (m, 1H, H2b), 2.17–2.03 (m, 1H, H6a), 2.00 (dd, J=13.4, 11.2 Hz, 1H, H6b); ^{13}C NMR (101 MHz, DMSO-d_6) δ 206.6 (C3), 175.2 (C7), 81.1 (C4), 73.3 (C1), 70.9 (C5), 47.9 (C2), 40.7 (C6). Characterization of product 44: ^{1}H NMR (400 MHz, DMSO-d_6) δ 4.26 (dd, J=3.7, 1.0 Hz, 1H, H4), 4.17 (dt, J=4.5, 3.0 Hz, 1H, H3), 2.94 (dd, J=13.9, 1.0 Hz, 1H, H6a), 2.50–2.46 (m, 1H, H6b), 2.36–2.27 (m, 1H, H2a), 2.17–2.03 (m, 1H, H2b); ^{13}C NMR (101 MHz, DMSO-d_6) δ 207.4 (C5), 174.2 (C7), 77.6 (C1), 77.1 (C4), 72.9 (C3), 49.1 (C6), 37.2 (C2).

Oxidation of 24-*epi*-brassinolide (45): *Epi*-brassinolide (**45**, 10.8 mg, 22 μmmol, 1 equiv.) was dissolved in DMSO-d_6 (0.5 mL) with one drop of D_2O in a NMR tube. A ^{1}H NMR spectrum was measured (d1=60) to determine the ratio of DMSO:starting material (DMSO was used as the internal standard). 1,4-Benzoquinone (2.8 mg, 26 μmol, 1.15 equiv.) and [(2,9-dimethyl-1,10-phenanthroline)Pd(μ-OAc)]$_2$(OTf)$_2$ (1, 0.6 mg, 0.6 μmol, 2.5 mol%) were added and the tube was shaken to form a homogeneous mixture. The mixture was left at room temperature for 6 h and then analyzed by NMR (^{1}H NMR: d1=60). Single and double oxidized products could not be distinguished by NMR, hence the conversion and selectivity of the oxidation is shown for each diol individually. Cyclic 2,3-*cis*-diol showed 55% conversion and 2-hydroxy-3-ketone as the main product (NMR yield 47%, selectivity of 85%). The selectivity was not 100% due to hydrate formation, overoxidation and or dimerization. Linear 22,23-diol showed 67% conversion and 22-hydroxy-23-ketone as the main product (NMR yield 67%, selectivity of 100%). The overall site-selectivities (calculated by dividing the NMR yield by 55+67=122% conversion) were 39% for oxidation at C3 and 55% at C23. Due to severe overlap not all NMR signals could be assigned. Only the assigned signals are reported: ^{1}H NMR (600 MHz, DMSO-d_6) δ 4.25 (dd, J=12.7, 6.0 Hz, 0.47H, 3-keto: H2), 4.22–4.18 (m, 0.47H, 3-keto: H7a), 4.17–4.10 (m, 0.45H, 45: H7a), 4.03 (s, 0.67H, 23-keto: H22), 3.91 (dt, J=12.8, 6.3 Hz, 1H, H7b), 3.74–3.70 (m, 0.45H, 45: H3), 3.55–3.49 (m, 0.47H, 3-keto: H5), 3.45–3.41 (m, 0.33H, 45: H22), 3.40 (ddd, J=12.2, 4.3, 2.6 Hz, 0.45H, 45: H2), 3.13 (t, J=5.4 Hz, 0.33H, 45: H23), 3.10–3.04 (m, 0.45H, 45: H5), 3.00 (t, J=13.5 Hz, 0.47H, 3-keto: H4a), 2.62 (p, J=6.8 Hz, 0.67H, 23-keto: H24), 2.29 (dd, J=13.0, 6.0 Hz, 0.47H, 3-keto: H1a), 2.07 (dd, J=14.7, 5.2 Hz, 0.47H, 3-keto: H4b), 1.76 (dq, J=13.5, 6.8 Hz, 0.76H, 23-keto: H25), 1.02 (s, 1.41H, 3-keto: H19). ^{13}C NMR (151 MHz, DMSO-d_6) δ 216.9 (23-keto: C23), 210.3 (3-keto: C3), 176.3 (45: C6), 174.3 (3-keto: C6), 79.0 (23-keto: C22), 75.5 (45: C23), 71.5 (45: C22), 70.2 (3-keto: C2), 69.9 (45: C7), 69.8 (3-keto: C7), 67.2 (45: C3), 67.1 (45: C2), 57.4 (45: C9), 55.7 (3-keto: C9), 52.5 (45: C17), 51.9 (23-keto: C17), 51.0 (45: C14), 49.4 (3-keto: C1), 48.5 (3-keto: C5), 46.8 (23-keto: C24), 42.1 (45: C13), 40.7 (45: C5), 39.3 (3-keto: C4), 39.1 (45: C8), 38.3 (3-keto: C10), 37.9 (45: C10), 37.8 (23-keto: C20), 30.7 (23-keto: C25), 26.4 (45: C25), 22.5 (45: C26/C27), 21.1 (23-keto: C26/27), 19.0 (23-keto: C26/27), 17.4 (45: C26/C27), 15.5 (45: C19), 15.3 (3-keto: C19).

Oxidation of 24-*epi*-castasterone (46): *Epi*-castasterone (**46**, 15.4 mg, 33 μmmol, 1 equiv.) was dissolved in DMSO-d_6 (0.5 mL) with one drop of D_2O in a NMR tube. A ^{1}H NMR spectrum was measured (d1=60) to determine the ratio of DMSO:starting material (DMSO was used as the internal standard). 1,4-Benzoquinone (3.9 mg, 36 μmol, 1.1 equiv.) and [(2,9-dimethyl-1,10-phenanthroline)Pd(μ-OAc)]$_2$(OTf)$_2$ (1, 0.8 mg, 0.8 μmol, 2.3 mol%) were added and the tube was shaken to form a homogeneous mixture. The mixture was left at room temperature for 8 h and then

analyzed by NMR (^{1}H NMR: d1 = 60). Single and double oxidized products could not be distinguished by NMR, hence the conversion and selectivity of the oxidation is shown for each diol individually. Cyclic 2,3-*cis*-diol showed 51% conversion and 2-hydroxy-3-ketone as the main product (NMR yield 42%, selectivity of 82%). The selectivity was not 100% due to hydrate formation, overoxidation and or dimerization. Linear 22,23-diol showed 66% conversion and 22-hydroxy-23-ketone as the main product (NMR yield 66%, selectivity of 100%). The overall site-selectivities (calculated by dividing the NMR yield by 51 + 66 = 117% conversion) were 36% for oxidation at C3 and 56% at C23. Due to severe overlap not all NMR signals could be assigned. Only the assigned signals are reported: ^{1}H NMR (600 MHz, DMSO-d_6) δ 4.18 (dd, J = 12.3, 6.7 Hz, 0.42H, 3-keto: H2), 4.04 (s, 0.66H, 23-keto: H3), 3.78–3.72 (m, 0.5H, 46: H3), 3.57–3.43 (m, 0.83H, 46: H2 + H22), 3.14 (t, J = 5.4 Hz, 0.34H, 46: H23), 2.74 (appt t, J = 13.6 Hz, 0.42H, 3-keto: H5), 2.66–2.55 (m, 1.45H, 46: H5 + 3-keto: H4a + 23-keto: H24), 2.18 (dd, J = 12.4, 6.8 Hz, 0.42H, 3-keto: H1a), 2.15–2.02 (m, 1.33H, 3-keto: H1b + H7 + 46: H7), 1.90–1.85 (m, 0.66H, 23-keto: H20), 1.81–1.71 (m, 0.66H, 23-keto: H25), 1.44–1.36 (m, 0.42H, 3-keto: H1b), 0.92 (s, 1.26H, 3-keto: H19). ^{13}C NMR (151 MHz, DMSO-d_6) δ 216.8 (23-keto: C23), 211.8 (46: C6), 210.7 (3-keto: C3), 208.9 (3-keto: C6), 79.0 (23-keto: C22), 75.5 (46: C23), 71.4 (46: C22), 71.4 (3-keto: C2), 67.5 (46: C3), 67.2 (46: C2), 57.2 (3-keto: C5), 51.9 (23-keto: C17), 51.9 (3-keto: C9), 50.5 (46: C5), 47.5 (3-keto: C1), 46.7 (23-keto: C24), 46.1 (46: C7), 45.7 (3-keto: C7), 42.4 (23-keto: C13), 42.4 (46: C13), 42.2 (3-keto: C10), 42.0 (46: C10), 40.6 (46: C24), 37.6 (23-keto: C20), 37.3 (3-keto: C8), 37.2 (46: C8), 35.9 (3-keto: C4), 30.6 (23-keto: C25), 26.4 (46: 25), 22.4 (46: C26/27), 21.0 (23-keto: C26/27), 18.9 (23-keto: C26/27), 17.4 (46: C26/27), 13.5 (3-keto: C19), 13.5 (46: C19).

General procedure of the competition experiments in DMSO-d_6 (Table S9-S10): A stock solution of the competing diol (**23-32**, 0.20 mL, 0.40 M in DMSO-d_6, 1 equiv.) was added to a stock solution of the benchmark diol (**23** or **24**, 0.20 mL, 0.40 M in DMSO-d_6, 1 equiv.) in a NMR tube. Next, a freshly made stock solution (0.20 mL) containing 1,4-benzoquinone (0.40 M in DMSO-d_6, 1 equiv.) and internal calibrant benzene (0.3-0.5 equiv.) was added. The NMR tube was shaken to obtain a homogeneous yellow mixture and a ^{1}H NMR was taken (t_0 measurement) with 16 scans (nt = 16) and a d1 value of 30 seconds (d1 = 30) prior to addition of the catalyst. Then a freshly made stock solution of [(2,9-dimethyl-1,10-phenanthroline)Pd(μ-OAc)]$_2$(OTf)$_2$ (1, 0.20 mL, 12 mM in DMSO-d_6, 3 mol%) was added. The final concentration of the diols was 0.10 M. The NMR tube was shaken again and the brown mixture was left overnight (16-24 h) at room temperature, after which ^{1}H NMR was measured again (t_1 measurement, d1 = 30). All competitions experiments were performed in duplicate.

Supporting Information

DFT calculations, synthesis of diol substrates, procedures for competition experiments, attempted alternative oxidation conditions, NMR spectra of the oxidation products and NMR spectra of competition experiments are available in the Supporting Information.[37–74]

Acknowledgements

The Dutch Research Council (NWO) is acknowledged for financial support. This work was partly sponsored by NWO-ENW for the use of supercomputer facilities (contract nr. 17197 7095). RWAH thanks S. Dolas (SURF, NL) for permission to perform calculations on the experimental ESC platform maintained and operated by SURF Open Innovation Lab. We thank the Center for Information Technology, University of Groningen, for support and access to the Peregrine high performance computing cluster. Prof. V. A. Khripach (National Academy of Sciences of Belarus) is acknowledged for the kind donation of 24-*epi*-brassinolide and 24-*epi*-castasterone.

Conflict of Interests

The authors declare no conflict of interest.

Data Availability Statement

The data that support the findings of this study are available in the supplementary material of this article.

Keywords: diols · oxidation · palladium · predictive model

[1] J. F. Hartwig, *Acc. Chem. Res.* **2017**, *50*, 549–555.
[2] J. Börgel, T. Ritter, *Chem* **2020**, *6*, 1877–1887.
[3] L. Guillemard, N. Kaplaneris, L. Ackermann, M. J. Johansson, *Nat. Chem. Rev.* **2021**, *5*, 522–545.
[4] M. S. Chen, M. C. White, *Science* **2010**, *327*, 566–571.
[5] P. E. Gormisky, M. C. White, *J. Am. Chem. Soc.* **2013**, *135*, 14052–14055.
[6] M. S. Chen, M. C. White, *Science* **2007**, *318*, 783–787.
[7] J. McIntyre, I. Mayoral-Soler, P. Salvador, A. Poater, D. J. Nelson, *Catal. Sci. Technol.* **2018**, *8*, 3174–3182.
[8] A. K. Cooper, D. K. Leonard, S. Bajo, P. M. Burton, D. J. Nelson, *Chem. Sci.* **2020**, *11*, 1905–1911.
[9] M. Valero, T. Kruissink, J. Blass, R. Weck, S. Güssregen, A. T. Plowright, V. Derdau, *Angew. Chem. Int. Ed.* **2020**, *59*, 5626–5631.
[10] D. S. Timofeeva, D. M. Lindsay, W. J. Kerr, D. J. Nelson, *Catal. Sci. Technol.* **2020**, *10*, 7249–7255.
[11] N. R. Conley, L. A. Labios, D. M. Pearson, C. C. L. McCrory, R. M. Waymouth, *Organometallics* **2007**, *26*, 5447–5453.
[12] R. M. Painter, D. M. Pearson, R. M. Waymouth, *Angew. Chem. Int. Ed.* **2010**, *49*, 9456–9459.
[13] K. Chung, S. M. Banik, A. G. De Crisci, D. M. Pearson, T. R. Blake, J. V. Olsson, A. J. Ingram, R. N. Zare, R. M. Waymouth, *J. Am. Chem. Soc.* **2013**, *135*, 7593–7602.
[14] K. Chung, R. M. Waymouth, *ACS Catal.* **2016**, *6*, 4653–4659.
[15] V. R. Jumde, N. N. H. M. Eisink, M. D. Witte, A. J. Minnaard, *J. Org. Chem.* **2016**, *81*, 11439–11443.
[16] M. Jäger, M. Hartmann, J. G. de Vries, A. J. Minnaard, *Angew. Chem. Int. Ed.* **2013**, *52*, 7809–7812.
[17] N. N. H. M. Eisink, M. D. Witte, A. J. Minnaard, *ACS Catal.* **2017**, *7*, 1438–1445.
[18] N. N. H. M. Eisink, J. Lohse, M. D. Witte, A. J. Minnaard, *Org. Biomol. Chem.* **2016**, *14*, 4859–4864.
[19] I. C. Wan, T. A. Hamlin, N. N. H. M. Eisink, N. Marinus, C. Boer, C. A. Vis, J. D. C. Codée, M. D. Witte, A. J. Minnaard, F. M. Bickelhaupt, *Eur. J. Org. Chem.* **2021**, *2021*, 632–636.
[20] S. Ramsay-Burrough, D. P. Marron, K. C. Armstrong, T. J. Del Castillo, R. N. Zare, R. M. Waymouth, *J. Am. Chem. Soc.* **2023**, *145*, 2282–2293.
[21] "The importance of sterics was further confirmed as a C4-THP protected glucoside oxidized fourfold less efficiently in competition experiments with unprotected glucosides. (see Ref. [17])," n.d..
[22] D. C. Ebner, J. T. Bagdanoff, E. M. Ferreira, R. M. McFadden, D. D. Caspi, R. M. Trend, B. M. Stoltz, *Chem. Eur. J.* **2009**, *15*, 12978–12992.
[23] I. V. Alabugin, K. M. Gilmore, P. W. Peterson, *Wiley Interdiscip. Rev.: Comput. Mol. Sci.* **2011**, *1*, 109–141.
[24] I. V. Alabugin, T. A. Zeidan, *J. Am. Chem. Soc.* **2002**, *124*, 3175–3185.
[25] M. Aufiero, R. Gilmour, *Acc. Chem. Res.* **2018**, *51*, 1701–1710.

[26] "See Supporting Information," **n.d.** see spectral data on page S292 and S329.
[27] "See Supporting Information for details, see spectral data on page S292 and S329.
[28] W.-J. van Zeist, F. M. Bickelhaupt, *Org. Biomol. Chem.* **2010**, *8*, 3118.
[29] F. M. Bickelhaupt, E. J. Baerends, *Rev. Comput. Chem.*, Wiley-VCH, New York **2000**, pp. 1–86.
[30] E. D. Glendening, A. E. Reed, J. E. Carpenter, F. Weinhold, *QCPE Bull.* **1990**, *10*, 58.
[31] J. P. Foster, F. Weinhold, *J. Am. Chem. Soc.* **1980**, *102*, 7211–7218.
[32] P. R. Rablen, R. W. Hoffmann, D. A. Hrovat, W. Thatcher Borden, *J. Chem. Soc. Perkin Trans. 2* **1999**, 1719–1726.
[33] D. R. Laplace, M. Van Overschelde, P. J. De Clercq, A. Verstuyf, J. M. Winne, *Eur. J. Org. Chem.* **2013**, 728–735.
[34] C. Le Sann, C. Abell, A. D. Abell, *Synth. Commun.* **2003**, *33*, 527–533.
[35] P. A. Bartlett, K. L. McLaren, M. A. Marx, *J. Org. Chem.* **1994**, *59*, 2082–2085.
[36] T. D. Goddard, C. C. Huang, E. C. Meng, E. F. Pettersen, G. S. Couch, J. H. Morris, T. E. Ferrin, *Protein Sci.* **2018**, *27*, 14–25.
[37] W. C. Ho, K. Chung, A. J. Ingram, R. M. Waymouth, *J. Am. Chem. Soc.* **2018**, *140*, 748–757.
[38] N. Marinus, N. Tahiri, M. Duca, L. M. C. M. Mouthaan, S. Bianca, M. van den Noort, B. Poolman, M. D. Witte, A. J. Minnaard, *Org. Lett.* **2020**, *22*, 5622–5626.
[39] T. Tanaka, N. Kikuta, Y. Kimura, S. Shoda, *Chem. Lett.* **2015**, *44*, 846–848.
[40] A. D. Becke, *J. Chem. Phys.* **1986**, *84*, 4524–4529.
[41] A. D. Becke, *Phys. Rev. A* **1988**, *38*, 3098–3100.
[42] S. Grimme, J. Antony, S. Ehrlich, H. Krieg, *J. Chem. Phys.* **2010**, *132*, 154104.
[43] A. D. Becke, E. R. Johnson, *J. Chem. Phys.* **2005**, *123*, 154101.
[44] E. Van Lenthe, E. J. Baerends, *J. Comput. Chem.* **2003**, *24*, 1142–1156.
[45] E. van Lenthe, E. J. Baerends, J. G. Snijders, *J. Chem. Phys.* **1993**, *99*, 4597–4610.
[46] E. van Lenthe, E. J. Baerends, J. G. Snijders, *J. Chem. Phys.* **1994**, *101*, 9783–9792.
[47] G. te Velde, F. M. Bickelhaupt, E. J. Baerends, C. Fonseca Guerra, S. J. A. van Gisbergen, J. G. Snijders, T. Ziegler, *J. Comput. Chem.* **2001**, *22*, 931–967.
[48] E. J. Baerends, http://www.scm.com, AMS2020..
[49] E. D. Glendening, C. R. Landis, F. Weinhold, *WIREs Comput. Mol. Sci.* **2012**, *2*, 1–42.
[50] E. D. Glendening, C. R. Landis, F. Weinhold, *J. Comput. Chem.* **2013**, *34*, 1429–1437.
[51] M. F. Guest, I. J. Bush, H. J. J. Van Dam, P. Sherwood, J. M. H. Thomas, J. H. Van Lenthe, R. W. A. Havenith, J. Kendrick, *Mol. Phys.* **2005**, *103*, 719–747.
[52] H. Ochiai, T. Niwa, T. Hosoya, *Org. Lett.* **2016**, *18*, 5982–5985.
[53] A. M. Esmurziev, N. Simic, B. H. Hoff, E. Sundby, *J. Carbohydr. Chem.* **2010**, *29*, 348–367.
[54] P. J. Card, G. S. Reddy, *J. Org. Chem.* **1983**, *48*, 4734–4743.
[55] W. Xu, S. A. Springfield, J. T. Koh, *Carbohydr. Res.* **2000**, *325*, 169–176.
[56] I. Jambal, K. Kefurt, M. Hlaváčková, J. Moravcová, *Carbohydr. Res.* **2012**, *360*, 31–39.
[57] L. A. Mulard, P. Kováč, C. P. J. Glaudemans, *Carbohydr. Res.* **1994**, *259*, 21–34.
[58] C. Aciro, T. D. W. Claridge, S. G. Davies, P. M. Roberts, A. J. Russell, J. E. Thomson, *Org. Biomol. Chem.* **2008**, *6*, 3751.
[59] T. Maki, S. Iikawa, G. Mogami, H. Harasawa, Y. Matsumura, O. Onomura, *Chem. Eur. J.* **2009**, *15*, 5364–5370.
[60] D. Viña, L. Santana, E. Uriarte, E. Quezada, L. Valencia, *Synthesis (Stuttg).* **2004**, *15*, 2517–2522.
[61] B. Hao, M. J. Gunaratna, M. Zhang, S. Weerasekara, S. N. Seiwald, V. T. Nguyen, A. Meier, D. H. Hua, *J. Am. Chem. Soc.* **2016**, *138*, 16839–16848.
[62] M.-Y. Hsu, Y.-P. Liu, S. Lam, S.-C. Lin, C.-C. Wang, *Beilstein J. Org. Chem.* **2016**, *12*, 1758–1764.
[63] K. C. Nicolaou, Y. He, K. C. Fong, W. H. Yoon, H.-S. Choi, Y.-L. Zhong, P. S. Baran, *Org. Lett.* **1999**, *1*, 63–66.
[64] S. Sakaguchi, D. Kikuchi, Y. Ishii, *Bull. Chem. Soc. Jpn.* **1997**, *70*, 2561–2566.
[65] J. M. William, M. Kuriyama, O. Onomura, *RSC Adv.* **2013**, *3*, 19247.
[66] J. M. William, M. Kuriyama, O. Onomura, *Adv. Synth. Catal.* **2014**, *356*, 934–940.
[67] M. Marx, T. T. Tidwell, *J. Org. Chem.* **1984**, *49*, 788–793.
[68] M. Lenze, E. B. Bauer, *Chem. Commun.* **2013**, *49*, 5889–5891.
[69] M. M. Hossain, S.-G. Shyu, *Tetrahedron* **2016**, *72*, 4252–4257.
[70] P. Bovicelli, P. Lupattelli, A. Sanetti, E. Mincione, *Tetrahedron Lett.* **1994**, *35*, 8477–8480.
[71] J. J. Dong, D. Unjaroen, F. Mecozzi, E. C. Harvey, P. Saisaha, D. Pijper, J. W. De Boer, P. Alsters, B. L. Feringa, W. R. Browne, *ChemSusChem* **2013**, *6*, 1774–1778.
[72] L. Chaveriat, I. Stasik, G. Demailly, D. Beaupère, *Tetrahedron: Asymmetry* **2006**, *17*, 1349–1354.
[73] C. T. Shei, H. L. Chien, K. Sung, *Synlett* **2008**, *7*, 1021–1026.
[74] H. M. Lui, Y. Sato, Y. Tsuda, *Chem. Pharm. Bull.* **1993**, *41*, 491–501.

Manuscript received: January 31, 2023
Accepted manuscript online: May 24, 2023
Version of record online: July 8, 2023